Development of a Spectroscopic Technique for Continuous Online Monitoring of Oxygen and Site-Specific Nitrogen Isotopic Composition of Atmospheric Nitrous Oxide*

Eliza Harris, David D. Nelson, William Olszewski, Mark Zahniser, Katherine E. Potter,
Barry J. McManus, Andrew Whitehill, Ronald G. Prinn and Shuhei Ono

MIT JOINT PROGRAM ON THE SCIENCE AND POLICY of GLOBAL CHANGE

*Reprinted from
Analytical Chemistry, 86(3): 1726–1734

Reprint 2014-6

The MIT Joint Program on the Science and Policy of Global Change combines cutting-edge scientific research with independent policy analysis to provide a solid foundation for the public and private decisions needed to mitigate and adapt to unavoidable global environmental changes. Being data-driven, the Program uses extensive Earth system and economic data and models to produce quantitative analysis and predictions of the risks of climate change and the challenges of limiting human influence on the environment—essential knowledge for the international dialogue toward a global response to climate change.

To this end, the Program brings together an interdisciplinary group from two established MIT research centers: the Center for Global Change Science (CGCS) and the Center for Energy and Environmental Policy Research (CEEPR). These two centers—along with collaborators from the Marine Biology Laboratory (MBL) at Woods Hole and short- and long-term visitors—provide the united vision needed to solve global challenges.

At the heart of much of the Program's work lies MIT's Integrated Global System Model. Through this integrated model, the Program seeks to: discover new interactions among natural and human climate system components; objectively assess uncertainty in economic and climate projections; critically and quantitatively analyze environmental management and policy proposals; understand complex connections among the many forces that will shape our future; and improve methods to model, monitor and verify greenhouse gas emissions and climatic impacts.

This reprint is one of a series intended to communicate research results and improve public understanding of global environment and energy challenges, thereby contributing to informed debate about climate change and the economic and social implications of policy alternatives.

Ronald G. Prinn and John M. Reilly,
Program Co-Directors

For more information, contact the Program office:
MIT Joint Program on the Science and Policy of Global Change

Postal Address:
Massachusetts Institute of Technology
77 Massachusetts Avenue, E19-411
Cambridge, MA 02139 (USA)

Location:
Building E19, Room 411
400 Main Street, Cambridge

Access:
Tel: (617) 253-7492
Fax: (617) 253-9845
Email: ***globalchange@mit.edu***
Website: ***http://globalchange.mit.edu/***

analytical chemistry

Article

pubs.acs.org/ac

Development of a Spectroscopic Technique for Continuous Online Monitoring of Oxygen and Site-Specific Nitrogen Isotopic Composition of Atmospheric Nitrous Oxide

Eliza Harris,*[†,‡] David D. Nelson,[§] William Olszewski,[†] Mark Zahniser,[§] Katherine E. Potter,[†] Barry J. McManus,[§] Andrew Whitehill,[†] Ronald G. Prinn,[†] and Shuhei Ono[†]

[†]Department of Earth, Atmospheric and Planetary Sciences, Massachusetts Institute of Technology, 77 Massachusetts Avenue, Cambridge, Massachusetts, 02139 United States

[‡]Laboratory for Air Pollution and Environmental Technology, Swiss Federal Institute for Materials Science and Technology (EMPA), Überlandstrasse 129, 8600 Dübendorf, Switzerland

[§]Atmospheric and Environmental Chemistry, Aerodyne Research Inc., 45 Manning Road, Billerica, Massachusetts, 01821 United States

Supporting Information

ABSTRACT: Nitrous oxide is an important greenhouse gas and ozone-depleting-substance. Its sources are diffuse and poorly characterized, complicating efforts to understand anthropogenic impacts and develop mitigation policies. Online, spectroscopic analysis of N_2O isotopic composition can provide continuous measurements at high time resolution, giving new insight into N_2O sources, sinks, and chemistry. We present a new preconcentration unit, "Stheno II", coupled to a tunable infrared laser direct absorption spectroscopy (TILDAS) instrument, to measure ambient-level variations in ^{18}O and site-specific ^{15}N N_2O isotopic composition at remote sites with a temporal resolution of <1 h. Trapping of N_2O is quantitative up to a sample size of ~4 L, with an optimal sample size of 1200–1800 mL at a sampling frequency of 28 min. Line shape variations with the partial pressure of the major matrix gases N_2/O_2 and CO_2 are measured, and show that characterization of both pressure broadening and Dicke narrowing is necessary for an optimal spectral fit. Partial pressure variations of CO_2 and bath gas result in a linear isotopic measurement offset of 2.6–6.0 ‰ mbar^{-1}. Comparison of IR MS and TILDAS measurements shows that the TILDAS technique is accurate and precise, and less susceptible to interferences than IR MS measurements. Two weeks of measurements of N_2O isotopic composition from Cambridge, MA, in May 2013 are presented. The measurements show significant short-term variability in N_2O isotopic composition larger than the measurement precision, in response to meteorological parameters such as atmospheric pressure and temperature.

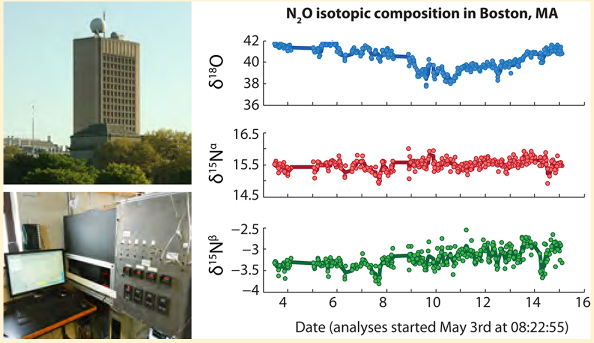

Nitrous oxide (N_2O) is a potent, long-lived greenhouse gas[1] and, as a source of reactive nitrogen to the stratosphere, the dominant contributor to catalytic ozone destruction in the 21st century.[2] Since preindustrial times, N_2O mixing ratio in the troposphere has increased from 270 ppb to the current level of 324.2 ± 0.1 ppb (2011) with an average growth rate of 0.2–0.3% yr^{-1} over the past decades.[3−5] This increase has been attributed to anthropogenic perturbation of the nitrogen cycle, in particular the application of inorganic fertilizers.[5−8] The N_2O budget, however, is poorly constrained due to the high spatial and temporal variability of fluxes, which limits our ability to develop targeted mitigation policies.[9,10]

Precise measurements of isotopologues of nitrous oxide (i.e., $^{14}N^{15}N^{16}O$, $^{15}N^{14}N^{16}O$, and $^{14}N^{14}N^{18}O$) provide a useful constraint to quantify contributions from different N_2O sources. [Site specific ^{15}N composition: $^{14}N^{15}N^{16}O = {}^{15}N^{\alpha}$ and $^{15}N^{14}N^{16}O = {}^{15}N^{\beta}$. Site preference in ^{15}N composition: SP $= {}^{15}N^{\alpha} - {}^{15}N^{\beta}$. Bulk ^{15}N composition: $(\delta^{15}N^{\beta} + \delta^{15}N^{\beta})/2 = {}^{15}N_{bulk}$. See Toyoda et al. (2013)[5] for a detailed account of isotope notation and terminology.] The major source of N_2O is microbial production in natural and agricultural soils, by both nitrifying and denitrifying bacteria. A number of studies have shown that the isotopic composition of N_2O can be used to distinguish between different microbial source pathways: The bulk ^{15}N composition of N_2O indicates the contribution of natural versus fertilized agricultural soil emissions,[7,11,12] while the site preference is independent of the reaction substrate and can be used to quantify different microbial processes, i.e.,

Received: October 30, 2013
Accepted: December 13, 2013
Published: December 13, 2013

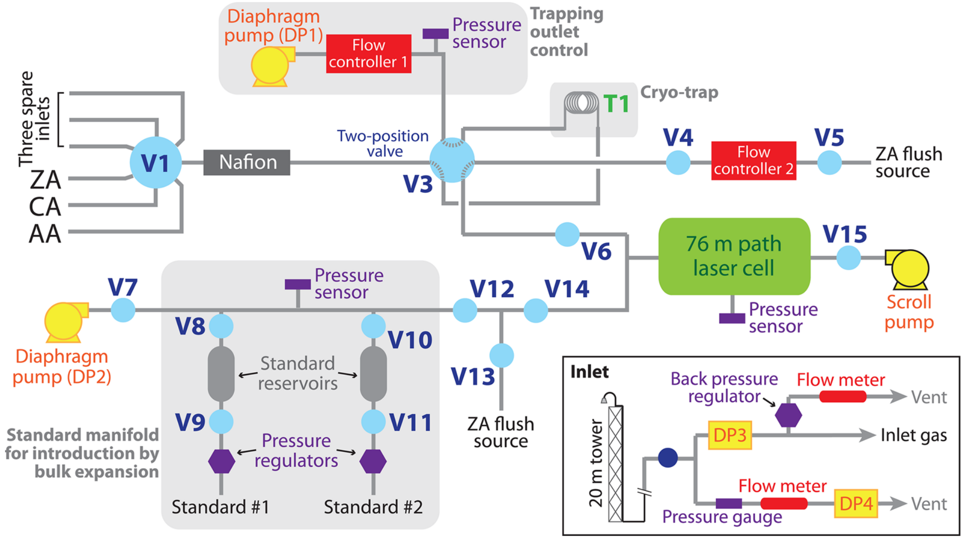

Figure 1. Schematic of the modified Medusa system "Stheno II", developed for preconcentration of N_2O without the use of chemical traps or liquid nitrogen. V specifies a valve, T is a trap, DP specifies a diaphragm pump, ZA = zero air, AA = ambient air, CA = compressed air. The instrument is shown with valve 3 in the "trapping" position. The system is described in detail in section S1 of the Supporting Information.

nitrification versus denitrification.[11−13] Relationships between $\delta^{15}N^{\alpha}$, $\delta^{15}N^{\beta}$, and $\delta^{18}O$ indicate the relative importance of N_2O reduction to N_2, and the oxygen isotopic composition also reflects the water in the environment where N_2O was formed.[14−17] In the troposphere, N_2O is stable, and the major sink is transfer to stratosphere, where N_2O is destroyed photolytically. UV photolysis is shown to produce a strong enrichment in $\delta^{18}O$ and $\delta^{15}N$ of the residual N_2O, in particular, the central position ^{15}N ($^{15}N^{\alpha}$).[18−20] This enrichment in $^{15}N^{\alpha}$ can be a particularly powerful tracer to quantify the magnitude of troposphere−stratosphere exchange, which is one of the largest uncertainties in the global N_2O budget.[21] The $\delta^{15}N$ and $\delta^{18}O$ composition of ambient N_2O shows a definite decreasing trend over the past decades, reflecting the increasing contribution of anthropogenic emissions, while observed trends in site preference remain inconclusive.[5,7,22,23]

Until recently, isotopic measurements of N_2O have used the traditional technique of flask sampling followed by laboratory-based isotope ratio mass spectrometry (IR MS). While this technique shows excellent precision for $\delta^{18}O$ and $\delta^{15}N$, it is unsuitable for field deployment, and continuous monitoring with high time resolution is technically challenging. In addition, site preference measurements are complicated by scrambling in the ion source, non-mass-dependent oxygen isotope composition, and mass interferences such as CO_2.[24−27] Unlike IR MS, tunable infrared laser direct absorption spectroscopy (TILDAS) measures fundamental rovibrational bands of nitrous oxide isotopologues in the midinfared regions at high precision; thus, the technique can be used to directly distinguish between $^{15}N^{\alpha}$ and $^{15}N^{\beta}$. TILDAS techniques have been applied to a number of isotopic systems such as CO_2 and O_3.[28,29] Several recent studies have shown the potential of TILDAS measurement coupled to a preconcentration unit for continuous, online measurement of N_2O isotopic composition.[30−33]

This study presents a new instrument that will be used to conduct online, real-time measurements of N_2O istopic composition at Mace Head Atmospheric Research Station, Ireland, as part of the AGAGE network (http://agage.eas.gatech.edu). A cryogen-free preconcentration unit with no chemical traps was developed to allow continuous, long-term monitoring at this remote site with minimal maintainance. For the first time, isotopic reference gases labeled for both $\delta^{18}O$ and site-specific $\delta^{15}N$ isotopic compositions were synthesized and measured with both IR MS and TILDAS. A comprehensive treatment of matrix dependence for TILDAS results is presented, as well as cross-calibration of site-specific isotope ratios against IR MS method, with an investigation of scrambling corrections for IR MS. Ambient air measurements and TILDAS to IR MS comparison show that TILDAS is both accurate and precise enough to observe ambient changes in $\delta^{18}O$, $^{15}N^{\alpha}$, and $^{15}N^{\beta}$ of N_2O with a temporal resolution of 0.5−2 h.

■ MATERIALS AND METHODS

Fully Automated Cryogen-Free N_2O Preconcentration. For N_2O preconcentration, we use a modified Medusa system[34] known as "Stheno II". [The "Stheno II" unit discussed here is a new unit, improving upon the principles used for the original "Stheno" preconcentration unit described in Potter et al. (2013).[35]] Medusa is a fully automated cryogen-free preconcentration unit coupled to GC/MS used to measure a number of CFCs and other non-CO_2 greenhouse gases at AGAGE stations;[34] a similar system has been used previously to preconcentrate N_2O for isotope measurements.[32,35] The preconcentration procedure involves collecting N_2O on a glass beads trap at approximately −156 °C and is described in detail in section S1 of the Supporting Information. Our system differs from previous preconcentration units used for spectroscopic measurements[31−33] in a number of ways; most notably, it uses a glass beads trap rather than a HayeSep D trap to adsorb N_2O, and CO_2 is not removed from the sample air stream. These changes allow long-term operation with minimal maintenance. A basic schematic of the preconcentration unit is shown in Figure 1, and an example of the preconcentration/trapping routine is presented in Figure 2.

Spectroscopic Analysis of N_2O Isotopic Composition with TILDAS. Spectroscopic measurements are made with a dual-laser TILDAS instrument (Aerodyne Research Inc.),

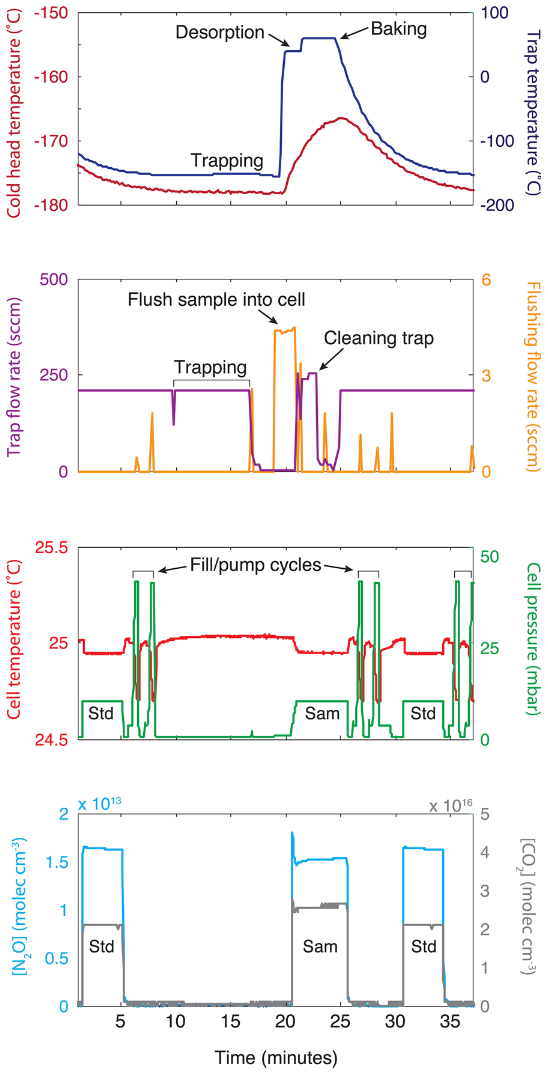

Figure 2. Trapping routine used for N_2O preconcentration on a liquid-nitrogen-free glass beads trap, coupled to TILDAS isotope measurement. The first panel shows the cold head (red) and trap (blue) temperatures. The second panel shows the flow rate through the trap (purple; both flush and sample) and the flushing flow used to push the sample into the laser cell (orange; spikes are due to multiport valve switching and do not affect measurement). The third panel shows the pressure (green) and temperature (red) in the laser measurement; the periods where the cell is cleaned are indicated, and Std refers to a standard while Sam refers to a sample. The fourth panel shows the concentration (molecules cm^{-3}) of N_2O (major isotope; blue) and CO_2 (gray) measured in the laser cell.

shown as the laser cell in Figure 1. The instrument has two lasers tuned to 2188 and 2203 cm^{-1} to measure the four isotopocules of N_2O, as shown in Figure 3. The spectroscopic measurements are described in detail in section S2 of the Supporting Information. Measurements are made at a pressure of 10 mbar with an N_2O mixing ratio of 65 ppm and a CO_2 mixing ratio of 8% (see section S2.2 in the Suppporting Information). Standards are run between every sample peak, as shown in Figure 2 (standards are discussed in section S2.4 in the Supporting Information). Following acquisition of the raw concentration data, corrections are made to account for background, matrix effects, and calibration to the international isotopic standard scale. The data analysis procedure and associated corrections are described in detail in section S2 of the Supporting Information, and an example of the data analysis cycle is shown in Figure S2 in the Supporting Information.

Synthesis of Standards by NH_4NO_3 Decomposition. A range of isotopic standards were synthesized via NH_4NO_3 decomposition to compare isotopic measurements between IR MS and TILDAS. The synthesis is described in detail in section S3 of the Supporting Information, and only a brief description will be given here. NH_4NO_3 with a range of isotopic compositions was produced from recrystallizing stock NH_4NO_3 with isotopic spikes of $Na^{15}NO_3$, $Na^{14}NO_3$, $^{15}NH_4Cl$, and $^{14}NH_4Cl$, as well as equilibration with $H_2{}^{18}O$. The NH_4NO_3 was flame-sealed into glass tubes and decomposed at 270 °C to form N_2O, which was purified by distillation with dry ice−ethanol and liquid nitrogen.[36] Five standards were produced with varying ^{15}N and ^{18}O compositions, as detailed in Table S2 in the Supporting Information.

Analysis of N_2O Isotopic Composition with Isotope Ratio Mass Spectrometry. Isotopic composition of N_2O standard gases was measured with IR MS (Thermo Electron MAT 253). Pure N_2O was used for analyses; gas chromatographic analysis with a thermal conductivity detector (TCD) showed no detectable CO_2 in N_2O samples derived from NH_4NO_3 decomposition (see Figure S6 in the Supporting Information). Following Toyoda and Yoshida (1999), N_2O^+ (masses 44, 45 and 46) and NO^+ (masses 30 and 31) ions were measured to determine position-specific ^{15}N substitutions.[25,27] Analysis conditions are summarized in Table S3 in the Supporting Information, and NO^+ ion scrambling factors are discussed in the sectinon describing Scrambling in the Ion Source in IR MS Analyses.

■ RESULTS AND DISCUSSION

Comparison of TILDAS and IR MS Measurements. The five N_2O standards synthesized by ammonium nitrate decomposition (Table S2 in the Supporting Information) as well as the two laboratory reference gases Ref I and Ref II were measured with IR MS and TILDAS in order to cross-calibrate the TILDAS and IR MS measured isotopologue ratios and investigate the accuracy of the two techniques considering IR MS scrambling factors and TILDAS matrix corrections. The results are presented in Table S4 in the Supporting Information and summarized in Figure 4, and show very good agreement between the IR MS and TILDAS for most samples. The instrument comparison shows that TILDAS is able to provide accurate results across a wide range of N_2O, CO_2, and bath gas compositions and N_2O isotopic compositions. TILDAS measurements at 23.5 and 40.5 ppm N_2O are not accurate: at $[N_2O]$ < approximately 45 ppm (at 0.010 atm, 1.7×10^{13} molecules cm^{-3}), peaks are too small for fitting (<4% absorption depth), and results are not accurate. Sufficient N_2O should be trapped to achieve at least 45 ppm in the cell at 0.010 atm, corresponding to ~1 L of air at a typical atmospheric N_2O mixing ratio of 327 ppb.

Matrix Effects on Spectroscopic Line Shape and Measurement Accuracy. The composition and pressure of the matrix has a significant effect on line shape, and thus on data fits and measurement accuracy. Samples (trapped ambient and compressed air) and standards are therefore matrix-matched as closely as possible. Measurement accuracy was tested across a

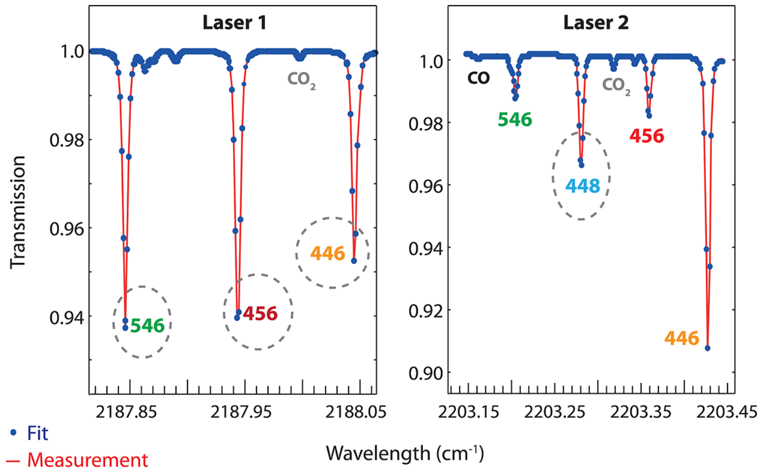

Figure 3. Measured (blue dots) and fitted (red line) spectra for laser 1 (2188 cm^{-1}) and laser 2 (2203 cm^{-1}). The peaks used for isotope measurements are circled with a gray dashed line. Measurement conditions: 8.9% CO_2, 69.5 ppm N_2O in synthetic air, P = 11.9 mbar, T = 298 K, path =76 m. The HITRAN lines and simulated (≡expected) spectra for the two lasers are shown in Figure S1in the Supporting Information for comparison with the measured and fitted spectra.

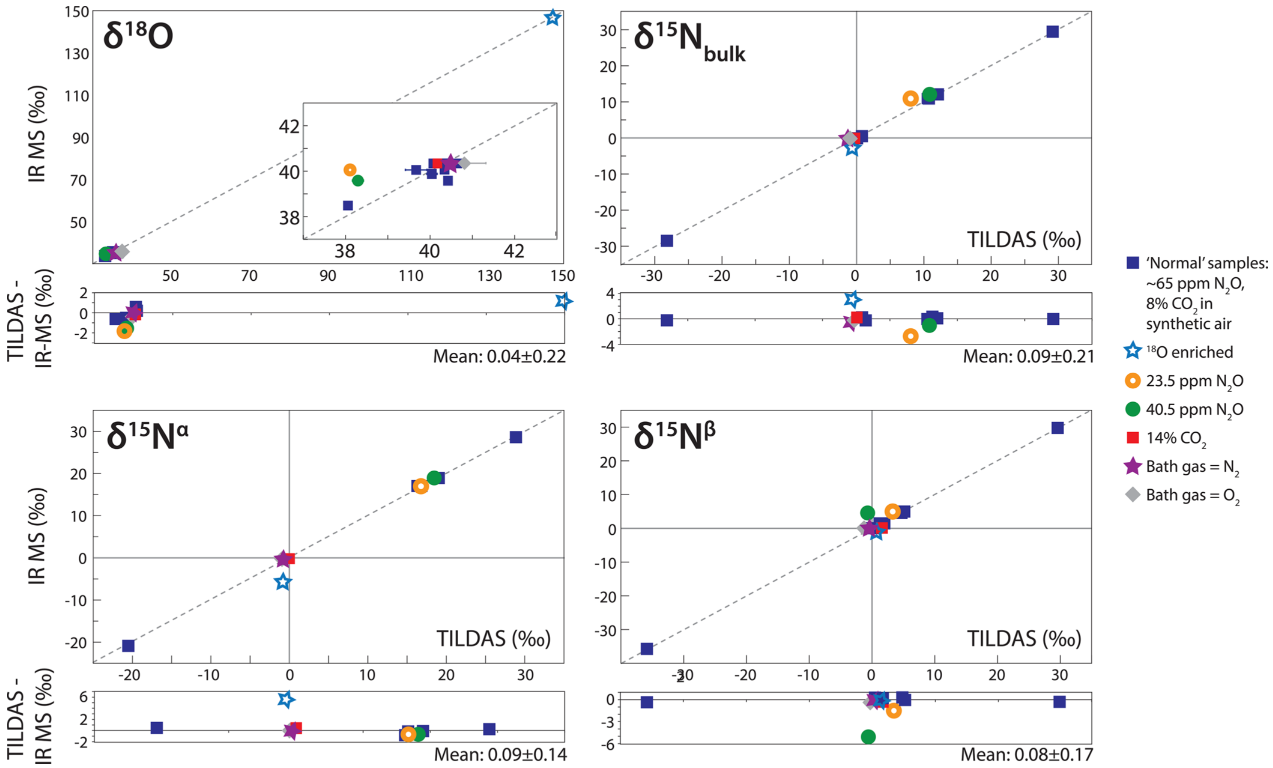

Figure 4. Comparison of N_2O isotope ratios measured with IR MS (y-axis) and TILDAS (x-axis) for the four isotopocules of N_2O. The offsets between the two techniques (TILDAS−IR MS) are shown under each plot. The exact values can be seen in Table S4 in the Supporting Information. The majority of samples were measured in the normal matrix (blue squares), but accuracy was tested across several matrix perturbations: low N_2O mixing ratio (yellow open and green filled circles), high CO_2 mixing ratio (red squares), and N_2 and O_2 bath gases (purple star and gray diamonds, respectively). ^{18}O enriched samples are indicated with open blue stars due to importance of ^{18}O composition when calculating site-specific ^{15}N composition of N_2O with IR MS.

range of matrix compositions. A brief description of the results is given here; full details are presented in section S2.4 of the Supporting Information. The primary matrix gas in the laser cell is zero air, hereafter referred to as the "bath gas"; the N_2:O_2 ratio of the bath gas does not have any significant effect on the peak shape (Figure S4 in the Supporting Information) or on measurement accuracy, as shown with measurements of Ref II in a bath gas of 100% N_2 and 100% O_2 (Figure 4). The total pressure of bath gas, on the other hand, has a significant effect on the results, affecting measured isotopic composition by

Table 1. Air-, Self-, and CO_2-Broadening Coefficients in cm^{-1} atm^{-1} for N_2O and CO_2 Peaks Measured by Varying Air (Bath Gas) Pressure between 0.0076 and 0.0113 atm and CO_2 Pressure between 0.0005 and 0.0013 atm[a]

		Lorentz width					
		γ_{air}				Doppler width	
molecule	peak position	HITRAN	this study	γ_{self} HITRAN	γ_{CO2} this study	β_{air}	β_{CO2}
$^{14}N^{14}N^{16}O$ (41)	2188.0448	0.0838	0.0858	0.110	0.0268	3.70	9.73
$^{14}N^{15}N^{16}O$ (42)	2187.9432	0.0798	0.0812	0.104	0.0409	4.05	16.56
$^{15}N^{14}N^{16}O$ (43)	2187.8460	0.0774	0.0837	0.101	0.0408	5.53	14.97
$^{14}N^{14}N^{18}O$ (44)	2203.2808	0.0774	0.0818	0.101	0.0286	4.84	11.91

[a] See Figure S7 in the Supporting Information. N_2O pressure was 5×10^{-7} atm; thus, self-broadening of N_2O was negligible during measurements. Molecule: numbers in brackets refer to the HITRAN identification number of the molecule. Peak positions are cm^{-1}.

~2.6−6 ‰ $mbar^{-1}$. The measurement pressure for standards is therefore regulated by the bulk expansion volume pressure (~750 mbar; section S2.2 in the Supporting Information) in the "standard reservoirs" shown in Figure 1, while the pressure for trapped sample measurements is controlled to within ±2% by the length of the flush into the cell (~90 s; section S1 in the Supporting Information and Figure 2). An empirical pressure correction is applied to account for the small differences in pressure that remain (±0.3 mbar; section S2.3 in the Supporting Information).

The CO_2 partial pressure affects the measurement accuracy with the same order of magnitude as the bath gas pressure (~2.6−4 ‰ $mbar^{-1}$; Table S1 and Figure S3 in the Supporting Information); however, it cannot be controlled in trapped samples as the ambient pressure of CO_2 shows significant temporal variation, for example >10% at Mace Head Station.[37,38] A pressure correction is therefore also applied to account for differences in CO_2 partial pressure, in addition to the pressure correction for bath gas pressure (section S2.3 in the Supporting Information). The empirically determined pressure dependencies are highly linear over the range of interest and show less than 5% change over longer time periods (section S2.4, Table S1 in the Supporting Information); therefore, they introduce <0.05‰ error under normal measurement conditions. Ref II was measured in a matrix with 14% CO_2 equivalent to an ambient mixing ratio of 700 ppm, requiring pressure corrections of −1.73 ± 0.09‰, 1.67 ± 0.08‰, and −2.56 ± 0.13‰ for $\delta^{15}N^{\alpha}$, $\delta^{15}N^{\beta}$, and $\delta^{18}O$, respectively. The pressure-corrected measurement showed very good agreement with IR MS and other TILDAS results, as shown in Figure 4 and Table S4 in the Supporting Information.

The pressure dependence of isotopic measurements is most likely caused by changes in peak shape and broadening in response to different matrix gases. Peak width in the TDL Wintel software used for spectroscopic data analysis (Aerodyne Research, Inc.) is described by an approximated Voigt profile, which can be deconvolved into contributions from the Gaussian Doppler line shape function and the Lorentz line shape function due to pressure broadening.[39] Both Gaussian and Lorentzian line widths were estimated as a function of pressure (see Figure S7 in the Supporting Information) by fitting measured spectra to a Voigt profile to find an optimum fit and exact width. The extent of pressure broadening and Dicke narrowing were estimated for comparison with literature values from the HITRAN database.[40,41] The measurements and calculations are presented in section S4 of the Supporting Information; the results will be described here. [Pressure is in units of atmospheres (atm) in this section for consistency with the HITRAN database.]

The parameters describing peak shape are summarized in Table 1. For all four N_2O peaks, it can be seen that the derived air broadening coefficients are consistently higher than given in the HITRAN database: ~2% for $^{14}N^{14}N^{16}O$ and $^{14}N^{14}N^{16}O$ (within the uncertainty of HITRAN data), 6% for $^{15}N^{14}N^{16}O$, and 8% for $^{14}N^{14}N^{18}O$ (significantly different to HITRAN data[42−44]). The HITRAN values for N_2O are measured at high pressures (>0.09 atm,[42,43]) relative to the pressures at which these measurements were made (~0.01 atm); more importantly, while the HITRAN line widths and strengths are taken from measurements of both $^{14}N^{14}N^{16}O$ and the minor isotopes, the HITRAN broadening coefficients are taken from measurements of only $^{14}N^{14}N^{16}O$.[42−44]

Although the estimate of Dicke-narrowing factor[45] (eq S7 in the Supporting Information) is based only on a parametrization and the effects of narrowing are expected to be largest at ~0.06−0.07 atm,[46] the results clearly show that there is significant narrowing at the low pressures used in the TILDAS cell. At measurement pressure of 10 mbar (0.01 atm), the Doppler width (2−2.3 cm^{-1} for the four N_2O peaks; see Figure S7 in the Supporting Information) contributes a large part of the total Voigt line width (2.4−2.8 cm^{-1}). Dicke narrowing has a significant impact on the Doppler width and the fit, accounting for ~50% of peak width change with pressure, and thus it is an important feature needed to gain accurate and precise results. We have implemented this narrowing into our fits and find a significant improvment in precision of repeated measurements on the order of 3−4×; e.g., precision on $\delta^{15}N^{\alpha}$ is 0.25−0.4‰ without the "Dicke factor" and improves to 0.07−0.15%‰ when the "Dicke factor" is included in the fit.

Scrambling in the Ion Source in IR MS Analyses. Site-specific N_2O isotopic composition is measured indirectly in the IR MS, by monitoring the isotopic composition of N_2O^+ ions (m/z = 44, 45, 46) and NO^+ ions (m/z = 30, 31). $^{15}NO^+$ ions result primarily from fragmentation of $^{14}N^{15}NO$; thus, the site-specific isotopic composition can be inferred.[24−26] This method is complicated by scrambling in the ion source, which means that ~8% of $^{15}NO^+$ is actually derived from $^{15}N^{14}NO$, and also relies on the assumption that the oxygen isotopic composition is mass-dependent.[27] This assumption is the reason why the site-specific isotopic composition for the 448-H sample, which is strongly enriched in ^{18}O, is poorly characterized with IR MS measurements, as shown in Figure 4: the directly measured value of $\delta^{18}O$ (mass 46) is used to infer $\delta^{17}O$ according to a mass-dependent relationship (eq 9 in the Supporting Information). The inferred $\delta^{17}O$ is then used to iteratively calculate site-specific ^{15}N isotopic composition from masses 45 ($^{15}N^{14}N^{16}O^+$, $^{14}N^{15}N^{16}O^+$, and $^{14}N^{14}N^{17}O^+$) and 31 ($^{15}N^{16}O^+$ and $^{14}N^{17}O^+$) (see eqs 10, 11, and 13 in the Supporting

Information). Thus, if the sample oxygen isotopic composition is not mass-dependent, the calculated values of $\delta^{17}O$ and thus site-specific N_2O isotopic composition are incorrect. In contrast, TILDAS is able to accurately measure site-specific ^{15}N substitutions across a large range of $\delta^{17}O$, $\delta^{18}O$, and $\Delta^{17}O$ values.

Scrambling in the ion source was considered by comparing the measured isotopic composition of the standards (not including 448-H), which have site preference values ranging from −1.76 to +15.09‰, between the IR MS and the TILDAS. Although the TILDAS values have an associated measurement error, the site-specific ^{15}N substitutions are directly measured; thus, there is no systematic relationship between site preference and error. Averaging across all the seven standards can therefore give an accurate view of IR MS measurement quality without a bias from TILDAS measurement uncertainty. The calculations used for the scrambling corrections (from refs 25, 27, 47) are presented in section S5 of the Supporting Information, and the results are summarized in Figure 5. Two possible scrambling models are considered: "one-factor" scrambling, with equal yield of $^{15}NO^+$ from $^{15}N^{14}NO$ and $^{14}NO^+$ from $^{14}N^{15}NO$ described by a single scrambling factor γ, i.e., γ of 0.08 means 8% of $^{15}NO^+$ is derived from $^{15}N^{14}NO$ and similarly for $^{14}NO^+$, and "two-factor" scrambling, where the scrambling of $^{14}N^{15}NO$ (γ^{α}) is not equal to the scrambling of $^{15}N^{14}NO$ (γ^{β}) (differences due to other isotopic substitution possibilities are not accounted for, e.g., clumped, ^{17}O, ^{18}O).

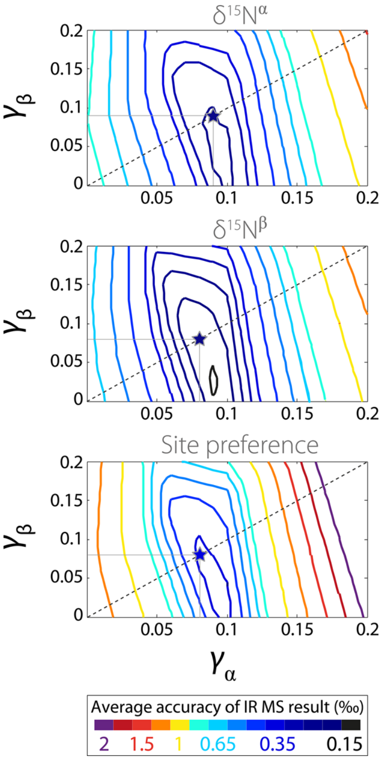

Figure 5. Absolute accuracy of site-specific N_2O isotopic measurements made with IR MS (defined as $|(\delta^{15}N^{\alpha})_{IRMS} - (\delta^{15}N^{\alpha})_{TILDAS}|$ averaged across the six N_2O standards, and similarly for $\delta^{15}N^{\beta}$ and site preference). Two-factor scrambling results are shown with the contour plot: γ^{α} (x-axis) shows the scrambling of $^{14}N^{15}NO$, and γ^{β} (y-axis) shows the scrambling of $^{15}N^{14}NO$. The lowest point of the contour plot shows the optimum scrambling factors. The dashed line indicates where both factors are equal, which is equivalent to the one-factor scrambling model. The star indicates where the deviation for the one-factor model is at a minimum (see Figure S8 in the Supporting Information for a full plot of one-factor scrambling results).

More complex scrambling models have also been considered;[27] however, the number of standards in this study is too small to consider the accuracy of models with a larger number of variables.

In agreement with the results of Westley et al.,[27] scrambling is more complex than a one-factor scrambling model can account for: The IR MS and TILDAS results never agree within the measurement error (Figure S8 in the Supporting Information) with the one-factor correction. Overall, best agreement is seen for one-factor scrambling with γ = 8%, consistent with results obtained using similar source conditions.[24,25,27] However, for calculation of $\delta^{15}N^{\alpha}$, best agreement is obtained with a scrambling factor of 9%, highlighting the limitations of the one-factor model.

The results from comparison of IR MS and TILDAS with two-factor scrambling show ~0.05‰ improvement in accuracy for the IR MS measurement compared to one-factor scrambling. The accuracy of results is much more sensitive to the scrambling of $^{14}N^{15}NO$ (γ_{α}) than $^{15}N^{14}NO$ (γ_{β}). From consideration of $\delta^{15}N^{\alpha}$, $\delta^{15}N^{\beta}$ and site preference, it is clear that the optimal value of γ_{α} is 8−9%, in agreement with previous studies,[24,25,27] while the optimal value of γ_{β} is clearly lower, between 2 and 4%. This value is much lower than reported by previous studies (e.g., single factor of 8.5% from Brenninkmeijer et al. 2009;[24] γ_{β} of ~9% from Westley et al. 2007[27]). This study presents the widest range of isotopic references gases yet considered and does not rely on primary calibration through techniques such as NH_4NO_3 decomposition or enriched gas mixing,[24,25,27,47] which give uncertainties of >0.2−0.3‰ in site preference, but instead presents the first laser spectroscopy-calibrated consideration of IR MS scrambling. The accuracy of standard site preference values in previous studies may not have been high enough to fully assess the optimum value of γ_{β}, considering that the calculated site preference is much less sensitive to the chosen value of γ_{β} than the value of γ_{α}.

Even with the optimized two-factor scrambling model, correcting for scrambling in the ion source introduces an error larger than the combined IR MS and TILDAS measurement uncertainty for both $\delta^{15}N^{\alpha}$ and site preference ($\delta^{15}N^{\beta}$ is accurate to within the measurement uncertainty). The error that is introduced depends on the site preference value of the N_2O being considered; therefore, both measurement precision and accuracy are affected. This limits the potential of IR MS measurements for high-precision monitoring of site-specific N_2O isotope ratios in lab and field studies, particularly at remote background sites like Mace Head where relevant changes in isotopic composition are very small.

Isotopic Measurements in Preconcentrated Samples. *Trapping Efficiency: Trace Gas Recovery.* Quantitative recovery of N_2O following trapping is critically important to prevent introduction of isotope fractionation by absorption/desorption processes.[48,49] Unlike previous instruments,[31−33] the Stheno II preconcentration unit (and the predecessor Stheno I[35]) uses a glass beads trap instead of the stronger HayeSep D adsorbent. The major advantage of the glass beads trap is that no N_2/O_2 is trapped from the air; thus, the bath gas is added as a flush with a known composition, making the pressure and matrix easier to accurately control. The range over which glass beads can efficiently trap N_2O was investigated by trapping increasing amounts of sample and comparing the measured and expected N_2O and CO_2 concentrations, as shown in Figure 6. N_2O is efficiently trapped when the sample volume is <4 L; CO_2 is efficiently trapped until ~2 L. It is desirable to use the minimum trapped volume, to conserve sample when measuring flask samples and to achieve the highest possible time resolution when making continuous ambient measurements; however, at N_2O mixing ratios <45 ppm (at 10 mbar total cell pressure) isotopic analysis is no longer accurate (see section describing Comparison of TILDAS and IR MS Measurements). The "optimal trapping range" is therefore 1200−1800 mL of ambient air. Within this range, N_2O recovery is >99%, and therefore, the fractionation introduced by trapping is negligible.

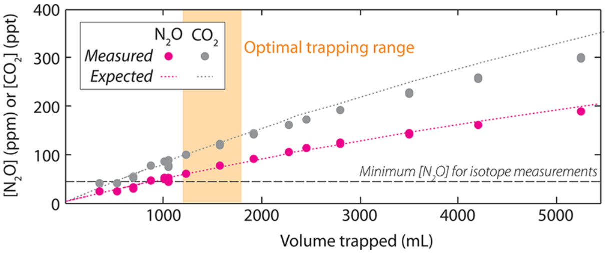

Figure 6. Measured (●) and expected (···) mixing ratios of N_2O and CO_2 as the volume of air trapped is increased from 400 to 5200 mL. The expected mixing ratio is curved with respect to volume trapped as the cell pressure also increases when a greater quantity of gas is trapped. The dashed line shows the minimum N_2O mixing ratio (at 10 mbar total cell pressure) required for accurate isotope analysis. Testing was performed with a flow rate of 370 sccm; further tests showed trapping efficiency is not affected by trapping flow rate up to 500 sccm.

Measurements of N_2O Isotopic Composition in Ambient Samples from Cambridge, Massachusetts. N_2O isotopic composition was measured continuously from MIT's "Green Building" for two weeks between March 3 and 16, 2013. The sampling inlet was located on the roof of the 18-story (95 m) building and connected to sampling pumps (see Figure 1) with >50 m of Synflex 1300 tubing (Eaton Corporation). Samples were measured every 28 min, and for every 5−10 ambient air samples, one compressed air sample (medical grade, Airgas Inc.) was measured to monitor trapping efficiency and precision. The compressed air measurements and precision histograms are shown in Figure S9 in the Supporting Information; the capabilities of the instrument are summarized in Table 2. Precision is better for $\delta^{15}N$ than $\delta^{18}O$ due to the relatively small absorption depth of the $^{14}N^{14}N^{18}O$ peak (Figure 3).

Ambient air measurements over the 13-day period are shown in Figure 7. The scatter in ambient air measurements ("true" variability + measurement error; bars in Figure 7 histograms) was compared to the scatter in compressed air measurements (measurement error only; smooth line in Figure 7 histograms), to determine if the instrument precision is sufficient to see changes in isotopic composition of ambient air. $\delta^{18}O$ values show a large amount of true variability over the measurement period; thus, although precision is lowest for this isotopocule, the precision is sufficient to observe ambient variations for both single measurement and four-point moving average. For $\delta^{15}N^{\beta}$, there is some true variability outside the measurement error with single measurements, although the difference between frequency distributions is much clearer for the four-point average data. The true variability is smaller than the measurement error of single measurements for both $\delta^{15}N^{\alpha}$ and $\delta^{15}N_{bulk}$; true variability of these isotopocules can only be resolved using the four-point moving average.

Table 2. Summary of the Precision Attainable with TILDAS Measurements of N_2O Isotopic Composition[a]

	$\delta^{18}O$	$\delta^{15}N^{\alpha}$	$\delta^{15}N^{\beta}$	$\delta^{15}N_{bulk}$
precision (‰), 28 min time resolution	0.32	0.17	0.19	0.16
$n_{averaged}$ for <0.2‰ precision	3	no averaging required		
temporal resolution (h)	1.4	0.5	0.5	0.5
$n_{averaged}$ for <0.1‰ precision	11	3	4	3
temporal resolution (h)	5.1	1.4	1.9	1.4

[a] "Precision" is the 1σ standard deviation of repeated measurements of compressed air. $n_{averaged}$ is the amount of measurements that need to be averaged to achieve a certain precision.

The isotopic measurements were compared to weather variables to examine causes of variability in isotopic composition. The weather data is shown in Figure S10 in the Supporting Information, and correlations are summarized in Table S5 in the Supporting Information. All four isotopomers show a significant relationship to pressure: a positive correlation for $\delta^{18}O$ and a negative correlation for all ^{15}N isotopomers. This correlation may relate to exchange of free tropospheric air. Relative humidity showed a significant correlation with all isotopocules except $\delta^{15}N^{\alpha}$. It is possible that this relates to partitioning between different microbial pathways. Wind direction showed a significant relationship to $\delta^{15}N^{\beta}$, with slightly isotopically heavier N_2O originating from the continent and isotopically light N_2O from the marine sector. A full investigation of the relationship between meteorological variables and measured isotopic composition is beyond the scope of this study and will be discussed in a later publication.

■ CONCLUSIONS

Measurement of N_2O isotopic composition has traditionally involved the collection of flask samples, which are then purified and measured with IR MS in a laboratory. While this technique has yielded interesting results, potential for investigations of seasonal cycles or changes in sources related to meteorology is limited by the feasible number and temporal resolution of samples. Using preconcentration without CO_2 removal followed by TILDAS, we have obtained sufficient precision with a four-point moving average of 28-min measurements to observe ambient remote-site changes in all the isotopocules of N_2O, and we have demonstrated accuracy across a wide range of isotopic composition and site preference values. The "Stheno II" instrument is automated and remotely operated, and uses very few consumables, to be well-suited for remote deployment at sites such as Mace Head Atmospheric Research Station.

The time series in Figure 7 shows that there is significant variability in N_2O isotopic composition on very short time scales. The data shows decoupling between ^{15}N and ^{18}O content of N_2O. Variability in $\delta^{18}O$ is larger than variability in $\delta^{15}N^{\beta}$, which is in turn greater than variability in $\delta^{15}N^{\alpha}$ and $\delta^{15}N$ bulk. The isotopic composition of N_2O reflects sources, sinks, and transport, and the rich data set that can be obtained from "Stheno II" provides constraints on these processes. In combination with inverse modeling and analysis of other trace

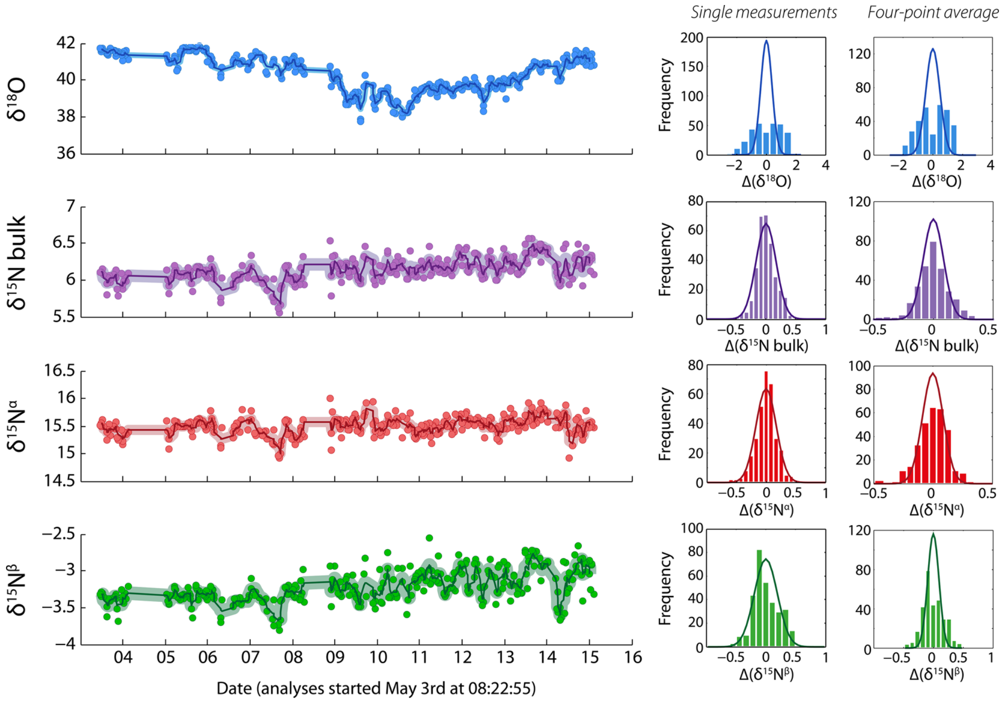

Figure 7. N_2O isotope ratios from repeated measurements of ambient air in Cambridge, MA. Left-hand panels show measured isotopic composition with time: points are individual measurements, and thick lines show the 4-point moving average. The thickness of the line corresponds to the 1σ error determined from repeated measurements of compressed air: 0.16‰, 0.08‰, 0.085‰, and 0.095‰ for $\delta^{18}O$, $\delta^{15}N_{bulk}$, $\delta^{15}N^{\alpha}$, and $\delta^{15}N^{\beta}$, respectively. Right-hand panels show the frequency distribution of deviations from the mean value in permil for single measurements and for four-point moving averages; i.e., $\Delta(\delta^{18}O) = \delta^{18}O_x$ - mean($\delta^{18}O$). Bars show the measured frequency distribution for ambient air measurements, while lines show the expected Gaussian distribution based on random error only, determined from repeated measurements of compressed air.

gases and meteorological variables, the results can be used to provide new insight into N_2O variability.

■ ASSOCIATED CONTENT

Ⓢ Supporting Information

Additional material as noted in text. This material is available free of charge via the Internet at http://pubs.acs.org.

■ AUTHOR INFORMATION

Corresponding Author

*E-mail: eliza.harris@empa.ch.

Notes

The authors declare no competing financial interest.

■ ACKNOWLEDGMENTS

We thank S. Toyoda and N. Yoshida at Tokyo Tech for calibration of reference N_2O, and S. O'Doherty, D. Young, and G. Spain for helpful suggestions regarding field deployment. We acknowledge NSF Grant 0959280 "MRI-R2: Development and Deployment of Automated Continuous Wave Quantum Cascade Laser Instruments for On-Site Monitoring of the Four Isotpomers of Nitrous Oxide" for supporting this work.

■ REFERENCES

(1) IPCC. In *Contribution of Working Group I to the Fourth Assessment Report of the Intergovernmental Panel on Climate Change*; Solomon, S., Qin, D., Manning, M., Chen, Z., Marquis, M., Averyt, K. B., Tignor, M., Miller, H. L., Eds.; Cambridge University Press: Cambridge, U.K., 2007.

(2) Ravishankara, A. R.; Daniel, J. S.; Portmann, R. W. *Science* **2009**, *326*, 123−125.

(3) Khalil, M. a. K.; Rasmussen, R. a.; Shearer, M. J. *Chemosphere* **2002**, *47*, 807−21.

(4) Park, S.; Croteau, P.; Boering, K. A.; Etheridge, D. M.; Ferretti, D.; Fraser, P. J.; Kim, K. R.; Krummel, P. B.; Langenfelds, R. L.; van Ommen, T. D.; Steele, L. P.; Trudinger, C. M. *Nat. Geosci.* **2012**, *5*, 261−265.

(5) Toyoda, S.; Kuroki, N.; Yoshida, N.; Ishijima, K.; Tohjima, Y.; Machida, T. *J. Geophys. Res.: Atmos.* **2013**, *118*, 1−13.

(6) Sowers, T.; Rodebaugh, A.; Yoshida, N.; Toyoda, S. *Global Biogeochem. Cycles* **2002**, *16*, 1129.

(7) Rockmann, T.; Kaiser, J.; Brenninkmeijer, C. A. M. *Atmos. Chem. Phys.* **2003**, *3*, 315−323.

(8) Wolf, B.; Zheng, X.; Brüggemann, N.; Chen, W.; Dannenmann, M.; Han, X.; Sutton, M. a.; Wu, H.; Yao, Z.; Butterbach-Bahl, K. *Nature* **2010**, *464*, 881−4.

(9) Nishina, K.; Akiyama, H.; Nishimura, S.; Sudo, S.; Yagi, K. *J. Geophys. Res.* **2012**, *117*, G04008.

(10) Cavigelli, M. A.; Grosso, S. J. D.; Liebig, M. A.; Snyder, C. S.; Fixen, P. E.; Venterea, R. T.; Leytem, A. B.; McLain, J. E.; Watts, D. B. *Front. Ecol. Environ.* **2012**, *10*, 537−546.

(11) Park, S.; Perez, T.; Boering, K. A.; Trumbore, S. E.; Gil, J.; Marquina, S.; Tyler, S. C. *Global Biogeochem. Cycles* **2011**, *25*, GB1001.

(12) Perez, T.; Trumbore, S. E.; Tyler, S. C.; Matson, P. A.; Ortiz-Monasterio, I.; Rahn, T.; Griffith, D. W. T. *J. Geophys. Res.: Atmos.* **2001**, *106*, 9869−9878.

(13) Sutka, R. L.; Ostrom, N. E.; Ostrom, P. H.; Breznak, J. A.; Gandhi, H.; Pitt, A. J.; Li, F. *Appl. Environ. Microbiol.* **2006**, *72*, 638−644.

(14) Yoshinari, T.; Wahlen, M. *Nature* **1985**, *317*, 349−350.

(15) Wahlen, M.; Yoshinari, T. *Nature* **1985**, *313*, 780−782.

(16) Ostrom, N. E.; Pitt, A.; Sutka, R.; Ostrom, P. H.; Grandy, A. S.; Huizinga, K. M.; Robertson, G. P. *J. Geophys. Res.: Biogeosci.* **2007**, *112*, G02005.

(17) Snider, D. M.; Venkiteswaran, J. J.; Schiff, S. L.; Spoelstra, J. *Global Change Biology* **2012**, *18*, 356−370.

(18) Rahn, T.; Zhang, H.; Wahlen, M.; Blake, G. A. *Geophys. Res. Lett.* **1998**, *25*, 4489−4492.

(19) Rockmann, T.; Kaiser, J.; Brenninkmeijer, C. A. M.; Crowley, J. N.; Borchers, R.; Brand, W. A.; Crutzen, P. J. *J. Geophys. Res.* **2001**, *106*, 10403−10410.

(20) Kaiser, J.; Engel, A.; Borchers, R.; Rockmann, T. *Atmos. Chem. Phys.* **2006**, *6*, 3535−3556.

(21) Park, S. Y.; Atlas, E. L.; Boering, K. A. *J. Geophys. Res.: Atmos.* **2004**, 109.

(22) Rahn, T.; Wahlen, M. *Global Biogeochem. Cycles* **2000**, *14*, 537−543.

(23) Röckmann, T.; Levin, I. *J. Geophys. Res.: Atmos.* **2005**, 110.

(24) Brenninkmeijer, C. A. M.; Röckmann, T. *Rapid Commun. Mass Spectrom.* **1999**, *13*, 2028−2033.

(25) Toyoda, S.; Yoshida, N. *Anal. Chem.* **1999**, *71*, 4711−4718.

(26) Kaiser, J.; Röckmann, T.; Brenninkmeijer, C. A. M. *J. Geophys. Res.* **2003**, *108*, 4476.

(27) Westley, M.; Popp, B. N.; Rust, T. M. *Rapid Commun. Mass Spectrom.* **2007**, *21*, 391−405.

(28) Weidmann, D.; Wysocki, G.; Oppenheimer, C.; Tittel, F. K. *Appl. Phys. B: Lasers Opt.* **2005**, *80*, 255−260.

(29) Janssen, C.; Tuzson, B. *Appl. Phys. B: Lasers Opt.* **2006**, *82*, 487−494.

(30) Uehara, K.; Yamamoto, K.; Kikugawa, T.; Yoshida, N. *Spectrochim. Acta, Part A* **2003**, *59*, 957−962.

(31) Mohn, J.; Guggenheim, C.; Tuzson, B.; Vollmer, M. K.; Toyoda, S.; Yoshida, N.; Emmenegger, L. *Atmos. Meas. Tech.* **2010**, *3*, 609−618.

(32) Mohn, J.; Tuzson, B.; Manninen, A.; Yoshida, N.; Toyoda, S.; Brand, W. A.; Emmenegger, L. *Atmos. Meas. Tech.* **2012**, *5*, 1601−1609.

(33) Köster, J. R.; Well, R.; Tuzson, B.; Bol, R.; Dittert, K.; Giesemann, A.; Emmenegger, L.; Manninen, A.; Cárdenas, L.; Mohn, J. *Rapid Commun. Mass Spectrom.* **2013**, *27*, 216−22.

(34) Miller, B. R.; Weiss, R. F.; Salameh, P. K.; Tanhua, T.; Greally, B. R.; Simmonds, P. G.; Mühle, J. *Anal. Chem.* **2008**, *80*, 1536−1545.

(35) Potter, K. E.; Ono, S.; Prinn, R. G. *Rapid Commun. Mass Spectrom.* **2013**, *27*, 1723−38.

(36) Potter, K. *Nitrous Oxide (N_2O) Isotopic Composition in the Troposphere: Instrumentation, Observations at Mace Head, Ireland, and Regional Modeling.* Ph.D. Thesis, Massachusetts Institute of Technology, 2011.

(37) Sirignano, C.; Neubert, R. E. M.; Rödenbeck, C.; Meijer, H. a. J. *Atmos. Chem. Phys.* **2010**, *10*, 1599−1615.

(38) Derwent, R.; Ryall, D.; Manning, A.; Simmonds, P.; O'Doherty, S.; Biraud, S.; Ciais, P.; Ramonet, M.; Jennings, S. *Atmos. Environ.* **2002**, *36*, 2799−2807.

(39) McManus, J. B.; Nelson, D. D.; Shorter, J.; Zahniser, M.; Mueller, A.; Bonetti, Y.; Beck, M.; Hofstetter, D.; Faist, J. *Proc. SPIE* **2002**, *4817*, 22−33.

(40) Rothman, L.; et al. *J. Quant. Spectrosc. Radiat. Transfer* **2009**, *110*, 533−572.

(41) Rothman, L. S.; Gamache, R. R.; Goldman, A.; Brown, L. R.; Toth, R. a.; Pickett, H. M.; Poynter, R. L.; Flaud, J. M.; Camy-Peyret, C.; Barbe, A.; Husson, N.; Rinsland, C. P.; Smith, M. a. *Appl. Opt.* **1987**, *26*, 4058−97.

(42) Nemtchinov, V.; Sun, C.; Varanasi, P. *J. Quant. Spectrosc. Radiat. Transfer* **2004**, *83*, 267−284.

(43) Toth, R. A. *J. Quant. Spectrosc. Radiat. Transfer* **2000**, *66*, 285−304.

(44) Lacome, N.; Levy, A.; Guelachvili, G. *Appl. Opt.* **1984**, *23*, 425−35.

(45) Demtroeder, W. *Laser Spectroscopy: Basic Principles*, 4th ed.; Springer-Verlag: Berlin, 2008; p 473.

(46) Tasinato, N.; Duxbury, G.; Langford, N.; Hay, K. G. *J. Chem. Phys.* **2010**, *132*, 044316.

(47) Kaiser, J.; Rockmann, T.; Brenninkmeijer, C. A. M.; Crutzen, P. J. *Atmos. Chem. Phys.* **2003**, *3*, 303−313.

(48) Bertolini, T.; Rubino, M.; Lubritto, C.; D'Onofrio, A.; Marzaioli, F.; Passariello, I.; Terrasi, F. *J. Mass Spectrom.* **2005**, *40*, 1104−8.

(49) Archbold, M. E.; Redeker, K. R.; Davis, S.; Elliot, T.; Kalin, R. M. *Rapid Commun. Mass Spectrom.* **2005**, *19*, 337−42.

MIT Joint Program on the Science and Policy of Global Change - REPRINT SERIES

FOR THE COMPLETE LIST OF REPRINT TITLES: http://globalchange.mit.edu/research/publications/reprints

2013-23 Probabilistic projections of 21st century climate change over Norther Eurasia, Monier, E., A. Sokolov, A. Schlosser, J. Scott and X. Gao, *Environmental Research Letters,* 8(4): 045008 (2013)

2013-24 Quantifying regional economic impacts of CO2 intenstity targets in China, Zhang, D., S. Rausch, V.J. Karplus and X. Zhang, *Energy Economics,* 40(2013): 687–701 (2013)

2013-25 Toward evaluating the effect of climate change on investments in the water resource sector: insights from the forecast and analysis of hydrological indicators in developing countries, Strzepek, K., M. Jacobsen, B. Boehlert and J. Neumann, *Environmental Research Letters,* 8(4): 044014 (2013)

2013-26 Modeling water resources within the framework of the MIT Integrated Global System Model: IGSM-WRS, Strzepek, K., A. Schlosser, A. Gueneau, X. Gao, É. Blanc, C. Fant, B. Rasheed and H.D. Jacoby, *Journal of Advances in Modeling Earth Systems,* 5(3): 638–653 (2013)

2013-27 Economic and emissions impacts of renewable fuel goals for aviation in the US, Winchester, N., D. McConnachie, C. Wollersheim and I.A. Waitz, *Transportation Research Part A: Policy and Practice,* 58(2013):116–128 (2013)

2013-28 An integrated assessment modeling framework for uncertainty studies in global and regional climate change: the MIT IGSM-CAM (version 1.0), Monier, E., J.R. Scott, A.P. Sokolov, C.E. Forest and C.A. Schlosser, *Geosci. Model Dev.* 6: 2063–2085 (2013)

2013-29 Characterization of the wind power resource in Europe and its intermittency, Cosseron, A., U.B. Gunturu and C.A. Schlosser, *Energy Procedia,* 40(2013): 58–66 (2013)

2013-30 Climate Change and Emissions Impacts on Atmospheric PAH Transport to the Arctic, Friedman, C.L., Y. Zhang and N.E. Selin, *Environmental Science & Technology,* online first, doi: 10.1021/es403098w (2013)

2013-31 Cost Concepts for Climate Change Mitigation, Paltsev, S. and P. Capros, *Climate Change Economics,* 4(Suppl.1): 1340003 (2013)

2013-32 Insights and issues with simulating terrestrial DOC loading of Arctic river networks, Kicklighter, D.W., D.J. Hayes, J.W. McClelland, B.J. Peterson, A.D. McGuire and J.M. Melillo, *Ecological Applications,* 23(8): 1817–1836 (2013)

2013-33 A Contemporary Carbon Balance for the Northeast Region of the United States, Lu X., D.W. Kicklighter, J.M. Melillo, P. Yang, B. Rosenzweig, C.J. Vörösmarty, B. Gross and R.J. Stewart, *Environmental Science & Technology,* 47(3): 13230–13238 (2013)

2013-34 European-Led Climate Policy versus Global Mitigation Action: Implications on Trade, Technology, and Energy, De Cian, E., I. Keppo, J. Bollen, S. Carrara, H. Förster, M. Hübler, A. Kanudia, S. Paltsev, R.D. Sands and K. Schumacher, *Climate Change Economics,* 4(Suppl. 1): 1340002 (2013)

2013-35 Beyond 2020—Strategies and Costs for Transforming the European Energy System, Knopf, B., Y.-H.H. Chen, E. De Cian, H. Förster, A. Kanudia, I. Karkatsouli, I. Keppo, T. Koljonen, K. Schumacher, D.P. van Vuuren, *Climate Change Economics,* 4(Suppl. 1): 1340001 (2013)

2013-36 Estimating regional methane surface fluxes: the relative importance of surface and GOSAT mole fraction measurements, Fraser, B., P.I. Palmer, L. Feng, H. Boesch, A. Cogan, R. Parker, E.J. Dlugokencky, P.J. Fraser, P.B. Krummel, R.L. Langenfelds, S. O'Doherty, R.G. Prinn, L.P. Steele, M. van der Schoot and R.F. Weiss, *Atmospheric Chemistry and Physics,* 13: 5697–5713 (2013)

2013-37 The variability of methane, nitrous oxide and sulfur hexaflouride in Northeast India, Ganesan, A.L., A. Chatterjee, R.G. Prinn, C.M. Harth, P.K. Salameh, A.J. Manning, B.D. Hall, J. Mühle, L.K. Meredith, R.F. Weiss, S. O'Doherty and D. Young, *Atmospheric Chemistry and Physics,* 13: 10633–10644 (2013)

2013-38 Integrated economic and climate projections for impact assessment, Paltsev, S., E. Monier, J. Scott, A. Sokolov and J.M. Reilly, *Climatic Change*, October 2013, doi: 10.1007/s10584-013-0892-3 (2013)

2013-39 Fiscal consolidation and climate policy: An overlapping generations perspective, Rausch, S., *Energy Economics,* 40(Supplement 1): S134–S148 (2013)

2014-1 Estimating a global black carbon emissions using a top-down Kalman Filter approach, Cohen, J.B. and C. Wang, *Journal of Geophysical Research—Atmospheres,* 119: 1–17, doi: 10.1002/2013JD019912 (2014)

2014-2 Air quality resolution for health impact assessment: influence of regional characteristics, Thompson, T.M., R.K. Saari and N.E. Selin, *Atmospheric Chemistry and Physics,* 14: 969–978, doi: 10.5194/acp-14-969-2014 (2014)

2014-3 Climate change impacts on extreme events in the United States: an uncertainty analysis, Monier, E. and X. Gao, *Climatic Change,* doi: 10.1007/s10584-013-1048-1 (2014)

2014-4 Will economic restructuring in China reduce trade-embodied CO_2 emissions? Qi, T., N. Winchester, V.J. Karplus, X. Zhang, *Energy Economics,* 42(March): 204–212 (2014)

2014-5 Assessing the Influence of Secondary Organic versus Primary Carbonaceous Aerosols on Long-Range Atmospheric Polycyclic Aromatic Hydrocarbon Transport, Friedman, C.L., J.R. Pierce and N.E. Selin, *Environmental Science and Technology,* 48(6): 3293–3302 (2014)

2014-6 Development of a Spectroscopic Technique for Continuous Online Monitoring of Oxygen and Site-Specific Nitrogen Isotopic Composition of Atmospheric Nitrous Oxide, Harris, E., D.D. Nelson, W. Olszewski, M. Zahniser, K.E. Potter, B.J. McManus, A. Whitehill, R.G. Prinn and S. Ono, *Analytical Chemistry,* 86(3): 1726–1734 (2014)

For limited quantities, Joint Program Reprints are available free of charge. Contact the Joint Program Office to order.

MIT Joint Program on
The Science and Policy of Global Change
Massachusetts Institute of Technology
77 Massachusetts Avenue, E19-411
Cambridge, MA 02139
USA